Robotic modules for a continuum manipulator with variable stiffness joints

Canberk Sozer, Sujit Kumar Sahu, Linda Paternò, *Member, IEEE*, and Arianna Menciassi, *Fellow Member*, *IEEE*

***Abstract*— This study presents a novel robotic module that combines rigid, rigid but compliant, and soft components to enable actuation, proprioceptive sensing, and variable stiffness. Three spring-reinforced soft actuators are employed for positioning the module in the 3D space by exploiting a ball joint as rotation center. Moreover, soft pads that are placed around the joint are used to tune the module stiffness regardless of the module position. Both actuation and stiffening are controlled by pressure, independently. Finally, the spring elements are used not only as reinforcement structures, but also as inductive sensors. Design, experimental characterization, and closed-loop control of the module are reported here. In addition, a multifunctional manipulator that is built by integrating three modules in a series is demonstrated. A specific architecture has been pursued to reduce the overall number of fluidic tubes required when adding a new module. It resulted in a manipulator with continuum soft actuators, but independent variable stiffness joints, which are the key feature for guaranteeing different bending angles of each segment.**

Results show that a single module can bend up to 30° omnidirectionally, its stiffness can increase up to 95% in a controllable way, and the output voltage change of the springs can be employed for position sensing. This design offers a highly compact, lightweight, and low-cost solution exploitable in a wide range of applications, from medical to rescue missions, where actions behind obstacles in highly confined areas are needed.

***Index Terms*— Soft Robot Materials and Design; Soft Sensors and Actuators; Actuation and Joint Mechanisms.**

I. INTRODUCTION

SOFT robotic manipulators are compliant structures that deform continuously, thus allowing for hyper-redundant degrees of freedom and high back-drivability [1]. These systems have attracted the interest of a lot of research groups [2]–[4]. Indeed, the inherent compliance of soft matter allows for safer physical interactions with the surroundings and higher adaptability even in unpredictable environments [2]. However, softness brings along small load-bearing capability and low positioning accuracy. Therefore, effective stiffness control strategies and rigid structural elements are usually needed to meet the requirements of real-world applications [1], [5], [6].

In this scenario, crustaceans pincers featured a rigid exoskeleton with inner soft muscles [7], and articulated human fingers with a rigid endoskeleton and external soft muscles [6] have offered two main inspiring biological references to design novel efficient manipulators which combine soft actuators with rigid structural components [6], [8]. Then, a soft pneumatic actuator within a continuum rigid exoskeleton [9], and two pneumatic soft actuators with a metallic hinge belt in the middle have been developed [10]. The rigid components act as reinforced elements of the pressurized soft actuators, enabling stiffness changes depending on the system configuration and bending motion in only one direction. For stiffness tuning without position dependency, active or semi-active solutions have been exploited [5]. Harsono et al. [11] combined pneumatic and cable-driven actuation antagonistically in a soft continuum manipulator with a rigid backbone structure based on spherical joints. The cables and rigid constraints allowed for bending the manipulator in any direction, while pneumatic soft artificial muscles were responsible for independent stiffness tuning. However, the exploitation of the same actuation technology for both functions (i.e., bending and stiffening) can allow for more compact and simple designs.

In this context, pneumatic actuation is one of the most widespread technologies for positioning and material stiffening in soft robotics [5], [12]. Vacuum-driven soft actuators have successfully demonstrated good capabilities in terms of force and displacement [13]. In addition, the jamming approach allows for switching from a very soft to a 40-fold stiffer body (e.g., from 0.2 to 7.8 N/mm [14]) by applying negative pressure within soft bags filled with granular, layer, and/or fiber materials [2], [5]. The main limitation is related to the achievable maximum stiffness depending on the applied negative pressure that cannot be less than 0.1 MPa [12], [15]. Therefore, recent works proposed a novel jamming concept based on positive pressurization to overcome this limit and potentially enable a wider stiffness range [15]–[17]. This approach exploits a pressurized soft actuator to compress and jam the granular, layer, and/or fiber materials contained in the soft jamming bag and increase the system stiffness. Hence, the main limitation has been shifted from the achievable pressure value to the material strength of the pneumatic soft actuator, allowing for more room for improvement. In particular, rigid structural elements [15] or inextensible fabrics [16] have been employed to constrain the soft actuator expansion in specific directions, decreasing the busting risk and focusing the generated compression force toward the jamming chamber.

Manuscript received: January 30, 2023; Revised: April 21, 2023; Accepted: June 5, 2023.

This paper was recommended for publication by Editor Yong-Lae Park upon evaluation of the Associate Editor and Reviewers' comments.

C. Sozer, S. K. Sahu, L. Paternò, and A. Menciassi are with The BioRobotics Institute, Scuola Superiore Sant'Anna, Pisa, Italy and with the Department of Excellence in Robotics & AI, Scuola Superiore Sant'Anna, Pisa, Italy.

We acknowledge the support of the BRIEF "Biorobotics Research and Innovation Engineering Facilities" project (Project identification code IR0000036) funded under the National Recovery and Resilience Plan (NRRP), Mission 4 Component 2 Investment 3.1 of Italian Ministry of University and Research funded by the European Union – NextGenerationEU.

Corresponding author: linda.paterno@santannapisa.it

Digital Object Identifier (DOI): see top of this page.

Similarly, the integration of a soft actuator within a rigid mechanical structure allows for stiffness tuning and locking mechanisms. In particular, the stiffness change is achieved through positive pressurization of the soft actuator that pushes on the rigid constraints and increases the friction at the soft-rigid interface, hindering the motion ability. This friction-based approach has been exploited to design variable stiffness hinges [18], [19], and continuum tubular mechanisms [20] with highly promising results, especially for applications that require high load capabilities in stiff configurations.

In this framework, we propose a novel pneumatic-driven module that combines spring-reinforced soft actuators with proprioceptive sensing in addition to a central rigid spherical joint that is able to change in stiffness without position dependency. The soft actuation in the 3D space ensures compliance and adaptability with the surroundings. At the same time, this hybrid soft-rigid design opens up new avenues for overcoming the challenges of fully soft robots in reaching high stiffness when necessary. Experimental characterization and closed-loop control of a module, as well as the demonstration of three serially integrated modules that enable a continuum manipulator with three independent variable stiffness joints are reported. The proposed technology can be exploited in various applications which require operating in very limited spaces for manipulation, exploration, search, and rescue, thus pushing the boundaries of robot abilities in many different fields.

II. Materials and Methods

A. Design Overview

The design and prototype of the proposed module are shown in Fig. 1a (Supplementary Video 1). The module is composed of a rigid structure, metallic but compliant springs, and soft chambers and pads (Fig. 1b). The final design is 35 mm in length and 17 mm in outer diameter with a 3 mm working channel at the center. The weight is 7 g and the material cost is less than 3 €.

The rigid structure is characterized by a passive spherical joint obtained by constraining a ball with an arm into a dedicated slot (Fig. 1c). Three caps are mechanically attached to the bottom part of the rigid structure, thus decreasing the circumference of the slot with the ball in the center. The top part of the rigid structure is coupled with the arm of the ball through a lateral extrusion and fixed on it. The final spherical joint can be bent between 0° and 30°, omnidirectionally. Three soft pads are integrated into equally spaced slots in the bottom rigid part, in a triangular configuration (Fig. 1c). Upon pressurization, the top membrane of the soft pads expands toward the ball joint and reduces its motion ability, resulting in stiffness enhancement. Only one pneumatic tube is required for controlling joint stiffness. Indeed, an inner open channel with one inlet and three outlets (yellow part in Fig. 1c) is designed into the bottom rigid part for distributing the input pressure from a single tube to the three pads, simultaneously.

Three soft actuators are obtained by integrating a soft chamber into a helical axial extension spring and equally placed around the spherical joint in a triangular configuration (Fig. 1a). When a soft chamber is pressurized, the spring limits the radial expansion but allows for elongation which results in omnidirectional bending thanks to the ball joint as rotation center (Fig. 1d). In particular, only one or two soft actuators can be pressurized simultaneously to bend the module. Indeed, the ball joint cannot elongate due to the mechanical constraints that prevent the ball from popping out of its slot. The three caps of the bottom part of the rigid structure ensure three mechanical constraints on the ball at the center (Fig. 1c).

In the presented design, the bending angle is limited between 0° and 30° by the rigid joint. However, the total bending angle can be increased by integrating multiple modules serially, as demonstrated later on (e.g., see Fig. 10). The springs are installed with a 10 mm pre-elongation when the module is at 0° initial position. It allows for the compression of the springs when the module is bent up to 30°, but avoids the short circuit between spring turns, which would compromise the sensing function. Indeed, the springs do not only limit the radial expansion of the pressurized soft chambers, but also behave as inductive sensors [21]. Indeed, elongation and compression of the springs cause a change in their inductance (L).

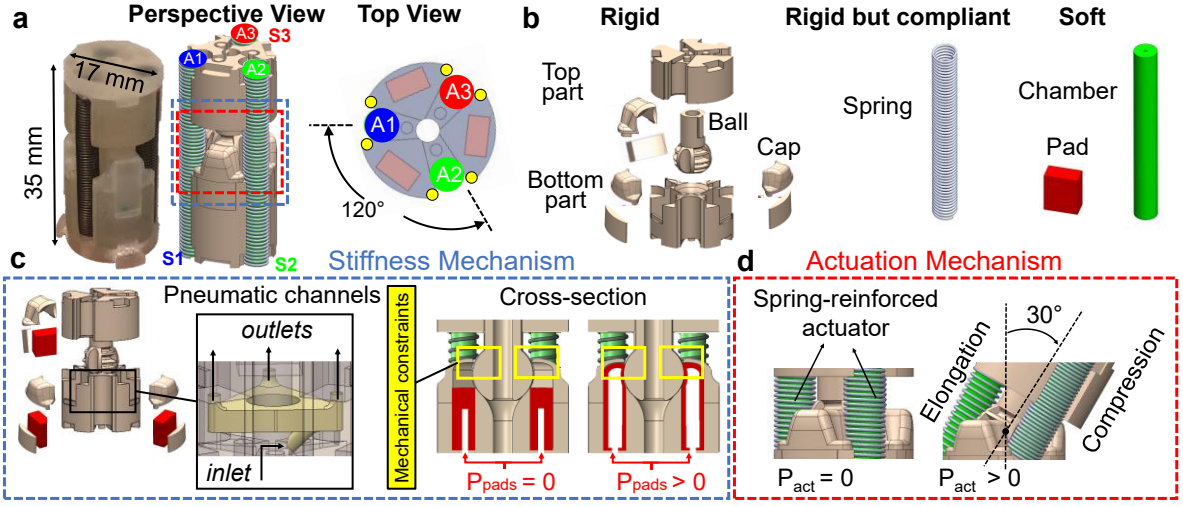

Fig. 1. (a) Prototype (left) and CAD (middle) of the module and (right) notation used for actuators and sensors: A1 = Actuator 1 with Sensor 1, A2 = Actuator 2 with Sensor 2, A3 = Actuator 3 with Sensor 3; (b) rigid, rigid but compliant, and soft components of the module; (c) variable stiffness and (d) actuation mechanisms of the module.

The output voltage (V_o) across the spring is inversely correlated to the spring length (l) when it is connected to a resistor (R) and an AC sinusoidal input voltage source of amplitude (V_i) in series. The voltage across the spring can be derived as follows:

$$V_o = \frac{\omega L}{\sqrt{R^2 + \omega^2 L^2}} \times V_i \quad (1)$$

where ω is the angular frequency of the input supply. Substituting $L = \frac{\mu_0 n^2 A}{l}$ in Eq. (1) and simplifying, we obtain:

$$V_o = \frac{a}{\sqrt{a^2 + l^2}} \times V_i \quad (2)$$

where $a = \frac{\omega \mu_0 n^2 A}{R}$. Since the permeability of free space (μ_0), the number of turns (n), the cross-sectional area (A) of the spring, and the angular frequency are considered constants, the coefficient a remains constant. Therefore, the output voltage decreases (increases) monotonically when the length of the spring increases (decreases). Therefore, the bending angle of the module can be estimated by measuring the output voltage of the three sensors, allowing for closed-loop control.

Different modules can be combined in a snake-like configuration to obtain a robotic manipulator. However, a main requirement for modular robots is minimizing the impact of the total number of modules (n) on both the central unit and single modules. As a result, a fundamental challenge in pneumatic systems is related to the number of tubes (N_t) that have to be integrated through the robot structure, from the central unit towards the modules [22]. In the proposed design, each module needs four tubes: three for actuation in the 3D space (spring-reinforced actuators), and one for stiffness tuning by inflating the three soft pads, simultaneously. Then, combining n modules requires the integration of $N_t = 4n$ tubes. This highly affects the development of a modular solution and limits the number of modules that can be combined. To address this challenge, the pneumatic tubes of the spring-reinforced actuators of the different modules can be serially integrated, thus obtaining a soft continuum manipulator with independent variable stiffness joints (Fig. 2). This architecture allows for a reduction in the total number of tubes from $N_t = 4n$ to $N_t = n+3$. Indeed, the final manipulator requires three tubes for the actuation, regardless of the module number, and a new module brings along just one new tube into the overall system for its stiffness tuning.

At the same time, the possibility to change the stiffness of each joint regardless of the position guarantees autonomous segments of the final system. Indeed, the motion freedom of each module can be controlled by tuning its stiffness. Thus, proper pressurization sequences of the actuators and variable stiffness mechanisms allow for different angles and directions of bending of each segment, despite the same bending actuators running along the entire manipulator. Finally, the bending motion of each segment can be re-adjusted on-line thanks to the integrated sensors of each module. Regarding the sensor cables coming from the springs, it has to be noted that they were selected as one-tenth in diameter with respect to fluidic tubes used in the design (i.e., 0.1 mm versus 1 mm) to minimize their effect on the more proximal modules.

In order to prevent mechanical interferences in the current design, a maximum of seven modules can be mounted, in series, since a maximum of six tubes can be integrated into the most proximal module (see Fig. 1a right: the six tubes that can be integrated into a module are shown by yellow circles). Additional modules can be integrated with changes to the current design to incorporate additional tubes by exploiting the central working channel or increasing the size of the module.

B. *Manufacturing*

Each spring-reinforced actuator consists of a soft chamber and a compliant metallic spring as a reinforcement element. The soft chamber is 27 mm in length and 3.3 mm in outer diameter with a central opening for inflation that is 0.65 mm in diameter. For their manufacturing, Ecoflex 00-50 silicone rubber (Shore Hardness: 00-50, Smooth-On, USA) was poured into a cylindrical mold with a rod in the center. Then, a pneumatic tube was fixed by using Sil-Poxy silicone glue (Smooth-On, USA), and the soft chamber was placed into the spring (Fig. 3a).

The spring (751-663, RS PRO, UK) is 4 mm in outer diameter, 0.36 mm in wire diameter, and 27 mm in length. It is made of steel (DIN17223 Class C), and its elastic constant for axial loads is given as 0.06 N/mm by the manufacturer.

The soft pads are 5 mm in length, 2.7 mm in width, and 6 mm in height with an opening of 1 mm in diameter and 4 mm in height at the center for inflation. They were manufactured by pouring Dragon Skin 10 silicone rubber (Shore Hardness: 10A, Smooth-On, USA) into a 3D printed mold (Fig. 3b).

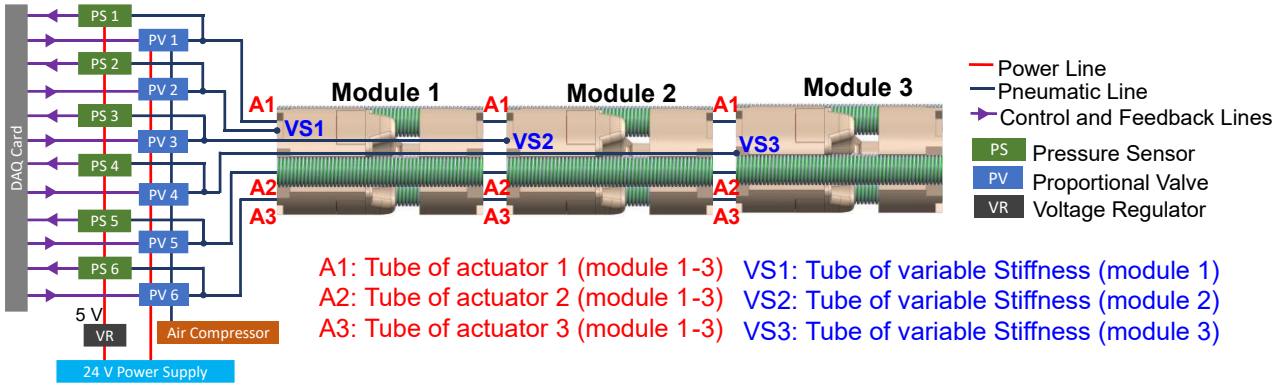

Fig. 2. System architecture of the soft continuum manipulator with variable stiffness joints. The figure is referred to n = 3 modules, which require 3 lines for independent stiffness and 3 lines for actuation. The maximum number of modules that can be integrated serially in the current design is n = 7, corresponding to 7 stiffening mechanisms. The tubes for actuators do not run along the manipulator, but they are attached at the bases of the most proximal module.

The rigid parts of the module and molds were 3D printed from UV-curable plastic material (VisiJet M3 Crystal, 3D Systems, USA). Subsequently, the spring-reinforced actuators and soft pads were integrated into the dedicated slots (Fig. 3c) and a tube for pressurizing the three soft pads simultaneously was glued to the inlet of the pneumatic channel (Fig. 1c) located in the bottom rigid part (Fig. 3d).

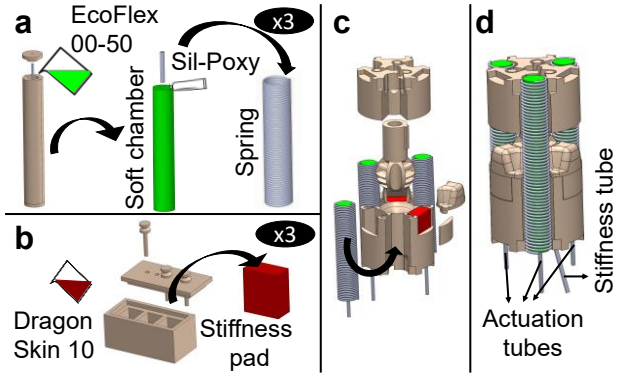

Fig. 3. Manufacturing of (a) the spring-reinforced actuators and (b) soft pads; (c) assembly of the module by integrating the spring-reinforced actuators and soft pads into the rigid structure; (d) final module.

C. *Experimental Setup*

A pressure control setup that can control up to three serially integrated modules was developed (Fig. 4a). Due to the selected architecture, the system has to control six pneumatic lines ($N_t = n+3$, where n = 3 modules), three for the soft continuum actuators and three for the variable stiffness joints (Fig. 2). The setup includes six proportional valves (Series K8P, Camozzi, Italy), and six pressure sensors (MPX5500DP, NXP Semiconductors, Netherland). A DAQ Card (USB-6363, National Instruments, USA) was controlled in LabVIEW to generate command signals for pressurizing actuators and pads, and to acquire signals from spring and pressure sensors.

III. Results and Discussion

A. *Actuation of the Module*

The workspace and the relationship between the input pressure and bending angle of the module were characterized by using an Aurora magnetic tracking system (Northern Digital, Canada), as shown in Fig. 4a.

The module prototype was fixed under the magnetic field generator at 0° initial position, and one actuator at a time was pressurized up to 200 kPa with a 1 kPa interval. A magnetic tracking probe was positioned on the module tip for recording its position. Fig. 4b and c show the workspace and pressure-bending angle results, respectively. Each curve in Fig. 4c reports the mean (solid line) and standard deviation (shaded area) of 5 trials. The maximum standard deviations were found as ±4.4°, ±4.3°, and ±4° for A1, A2, and A3, respectively. The maximum bending angle (i.e., 30°) was achieved by A1 at 120 kPa input pressure. On the contrary, A2 and A3 reached a bending angle of 27° at 130 kPa and maintained it, although the pressure was increased up to 200 kPa. This may be due to manufacturing inaccuracies.

The second actuation test investigated the output force in different directions at 0° and 30° configurations by using a Nano 43 load cell (ATI Industrial Automation, USA) (Fig. 5). The load cell was placed next to the module tip, opposed to the movement direction, and then one and two actuator(s) were pressurized up to 200 kPa with a 1 kPa interval, in the following order: A1, A2, A3, A1-A2, A1-A3, and A2-A3. The results measured at 0° and 30° are reported in Fig. 5a–f and Fig. 5g–l, respectively. Each graph consists of the mean (solid line) and standard deviation (shaded area) of 5 trials. Experimental results showed that the pressurized actuator(s) generated similar forces with slight variations. The mean and standard deviation of the maximum force resulted equal to 0.52 ± 0.07 N and 0.54 ± 0.04 N for the 0° and 30° initial positions at 200 kPa input pressure, respectively. The maximum standard deviation of the tests was found as 0.07 N.

B. *Proprioceptive Sensing of the Module*

Experimental tests were carried out to define a relationship between bending angle and output voltage across the three sensors. The sensor outputs were investigated by connecting each spring to an 82 Ω resistor and an AC sinusoidal voltage source in series (Fig. 6a). A function generator (33220A, Agilent Technologies, USA) was used to supply an AC sinusoidal waveform with a 5 V peak-to-peak voltage at 4.5 MHz. The peak-to-peak output voltage across the sensors was acquired at a sampling rate of 2 Giga Samples/s by an oscilloscope (MSO7034B, Agilent Technologies, USA).

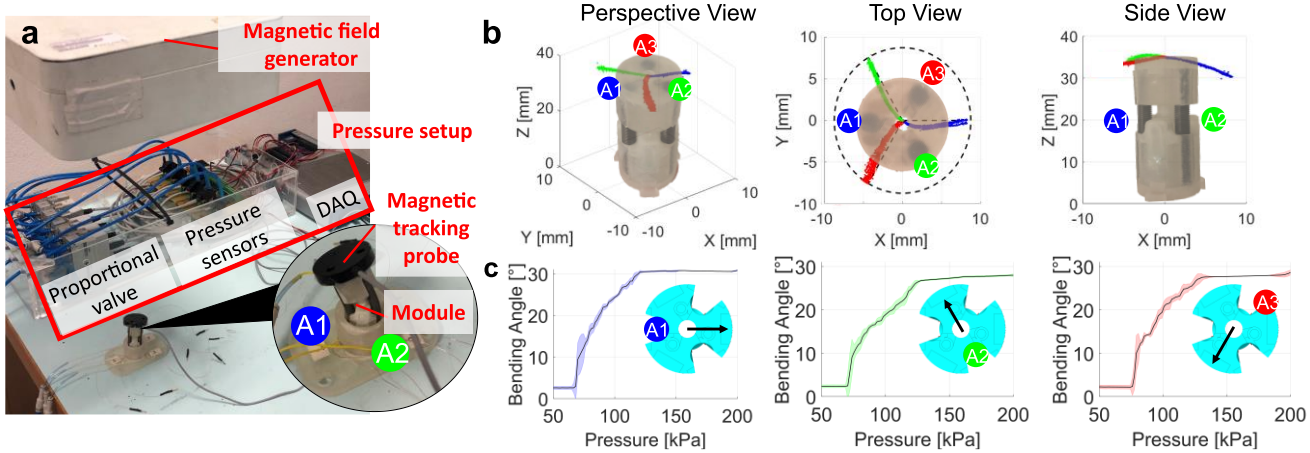

Fig. 4. (a) Setup for tracking the module tip; (b) module tip workspace in the 3D space; (c) mean (solid line) and standard deviation (shaded area) of bending angle with respect to the input pressure (5 trials for each test). The arrows represent the bending directions.

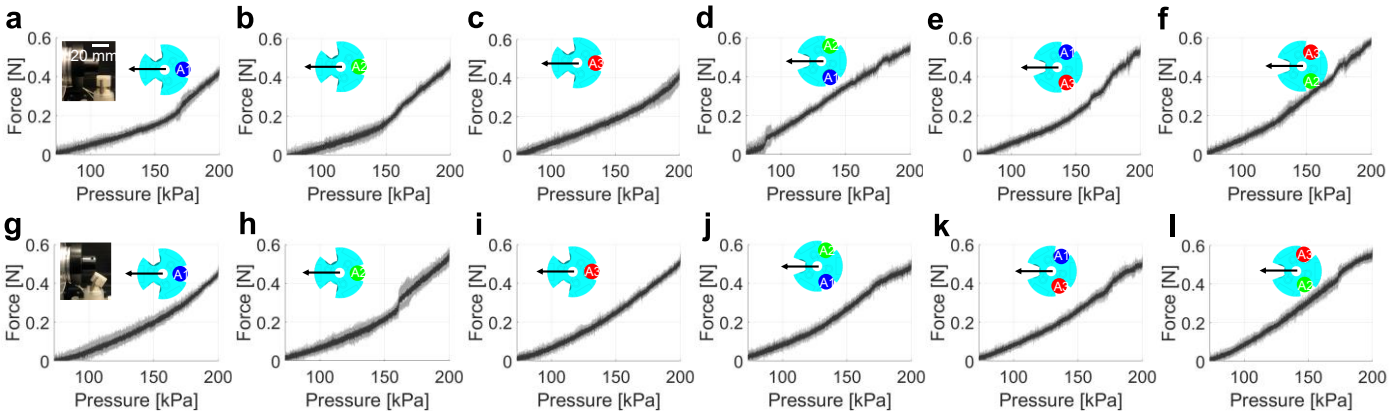

Fig. 5. Experimental results of the output force while the joint was at 0° (a-f) and 30° (g-l) initial positions. The mean (solid line) and standard deviation (shaded area) of 5 trials are reported. The arrows show the direction of force generation.

The tests started with the joint at 0° initial position. Then, one actuator at once was pressurized to bend the module up to 30°. In particular, A1, A2, and A3 were pressurized up to 120 kPa, 130 kPa, and 130 kPa, respectively, due to the previous experimental results obtained by the tracking set-up (Fig. 4). A pressure interval of 1 kPa was used during tests. This was repeated 5 times for each actuator. The bending angle from Aurora, the output voltage of the springs from the oscilloscope, and the input pressure were recorded by LabVIEW, synchronously.

Fig. 6c–e show the outputs of the sensors S1, S2, and S3 while A1, A2, or A3 were pressurized up to 120 kPa, 130 kPa, and 130 kPa, respectively. A power curve was fitted on the results of the 5 trials, thus defining the correlation between the bending angle and the output voltage of the sensors.

Sensor output results showed that the initial voltage of each spring at the initial position shows some differences. At 0°, the mean and standard deviation of the voltage of S1, S2, and S3 were 3107 ± 7 mV, 3089 ± 7 mV, and 3152 ± 2 mV, respectively. The difference could be a result of inaccuracies in the manual fabrication of the spring-reinforced actuators.

When the module is at 30°, experimental results showed that the output voltage of a sensor decreases by 3.1% on average in elongation (~ 95 mV) and increases by 2.2% on average in compression (~ 68 mV). This change is sufficient to be correlated with the bending angle of the module.

C. *Closed-Loop Control of the Module*

A PI controller (K_P = 0.1 and K_I = 0.01) was designed for closed-loop control of the module position. As a preliminary demonstration, the closed-loop control was verified in the *xz* plane (Fig. 4b) by using the calibration curve of S1 sensor (blue curve in Fig. 6c). A1 actuator was pressurized to bend the joint toward +*x* direction, and A2 and A3 actuators were pressurized together to bend it toward -*x* direction. A step reference signal was set in LabVIEW from 0° to 30° back and forth with a 5° interval, each step for 10 seconds (*Step Reference* in Fig. 7).

The angle estimated by S1 (*Sensor Response* in Fig. 7) was compared to the angle measured by image-based ground truth data (*Ground Truth* in Fig. 7) (Supplementary Video 2). In the video, the response of the module following random step references is demonstrated also against external disturbances (applied by the pen in the video). In Fig. 7, it can be observed that the module was able to reach the desired bending angle by only performing oscillations thanks to the information coming from S1 sensor. It was also observed from 0 to 60 s that the closed-loop control response of the module matched the reference signal with a mean rise and settling time of 0.63 s and 2.56 s, respectively. The maximum and mean difference between ground truth and angle estimated from S1 were found less than 2° and 0.44°, respectively. In the future, this error could be reduced by a more sophisticated control system design.

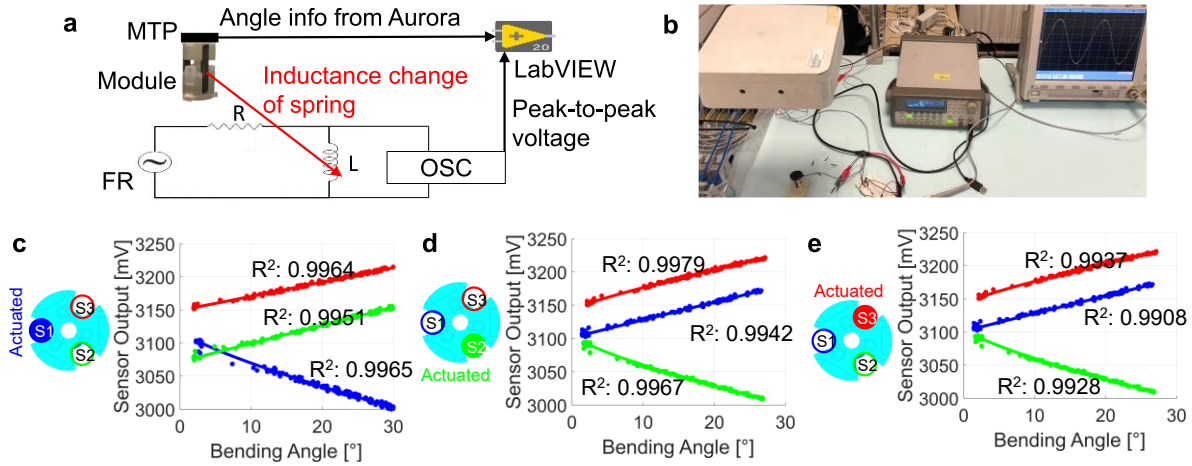

Fig. 6. (a) Circuit diagram and (b) experimental setup for measuring the sensor outputs, bending angle, and input pressure simultaneously. Sensor outputs when (c) A1, (d) A2, and (e) A3 actuators were pressurized one by one. The tests were repeated 5 times and the results are given together with the fitted curve and R^2 value. In (a) FR: Function Generator; R: Resistor; L: Inductor (Spring); OSC: Oscilloscope; MTP: Magnetic Tracking Probe.

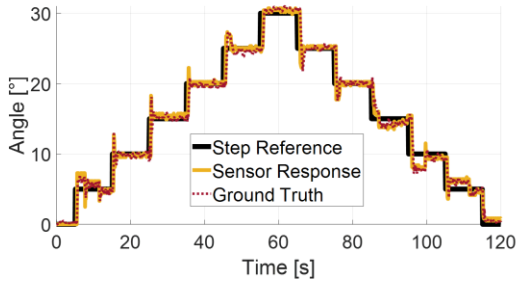

Fig. 7. Step reference signal (black) compared with the angles estimated by S1 (yellow) and by an image-based ground truth (dashed red line).

D. Variable Stiffness of the Module

The proposed variable stiffness method relies on reducing the motion ability of the ball joint by pressurizing the soft pads and filling the cavities of the rigid structure around the central ball. Therefore, two different ball geometries were tested to investigate how the stiffness may be affected by the design of the contact area between the soft (i.e., soft pads of Dragon Skin 10 silicone rubber, shore hardness: 10A, Smooth-On, USA) and rigid (i.e., 3D printed ball joint of UV curable plastic material VisiJet M3 Crystal, 3D Systems, USA) materials. The first ball joint had a flat geometry with a surface area of 173 mm^2, while the second one had dents that increase the surface area to 255 mm^2 (Fig. 8).

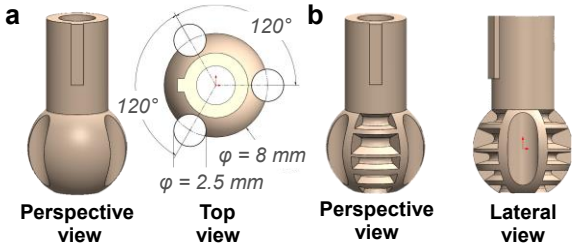

Fig. 8. (a) Design of the flat surface ball joint and (b) design of the same ball joint with dents that allow for an increment in the surface area. Φ: diameter.

A Nano 43 load cell was attached to an RV-3SB robot arm (Mitsubishi Industrial Robot, Japan), and it was placed next to the tip of the module that is positioned at 0° straight configuration. Then, the soft pads were pressurized, and the force sensor was pushed 3 mm at 5 mm/s speed. It was repeated 5 times for both the ball joints with the flat surface and the one with dents. For the input pressure of the soft pads, the range was set between 0 and 500 kPa to avoid the breakdown of the plastic rigid structure [18]. However, during these tests, the stiffness was measured only at 300 kPa, since they aimed at investigating the best design of the ball joint. Further pressure values have been analyzed in the final design.

The force data were divided by the displacement (i.e., 3 mm) to calculate the stiffness, which resulted in 0.142 ± 0.005 N/mm for the ball joint with the flat surface and 0.195 ± 0.007 N/mm for the ball joint with dents. Since the results showed that the stiffness was 38% higher for the ball joint with dents, it was selected for the final design, and further tests were carried out to characterize the variable stiffness properties of the final module. Then, the soft pads were pressurized up to 500 kPa with a 100 kPa interval. A force sensor was placed next to the module tip and pushed 3 mm at 5 mm/s speed (the directions for each configuration are shown with white arrows in Fig. 9) while the soft pads were pressurized. This process was carried out in different configurations: (*i*) when the module was at 0° (Fig. 9a), (*ii*) when the module was at 30° with A1 actuator pressurized (Fig. 9b), and (*iii*) when the module was at 30° with A2 and A3 pressurized simultaneously (Fig. 9c). Each configuration was tested 5 times. The collected force data were divided by the displacement (i.e., 3 mm). The mean and standard deviation are given in Fig. 9a–c. As expected, at 0 kPa input pressure of the soft pads, the stiffness of the module was higher when spring-reinforced actuators were pressurized (i.e., 0.12 N/mm when no actuator was pressurized, 0.14 N/mm when A1 was actuated, 0.31 N/mm when A2 and A3 were actuated simultaneously). Indeed, the pressurized actuators increase the module stiffness, as well.

When the soft pads were pressurized at 500 kPa, the stiffness of the module increased by 95%, 81%, and 79% at the initial positions of 0°, 30° with A1 pressurized, and 30° with A2 and A3 pressurized simultaneously, respectively. The maximum standard deviation was calculated as ± 0.03 N/mm.

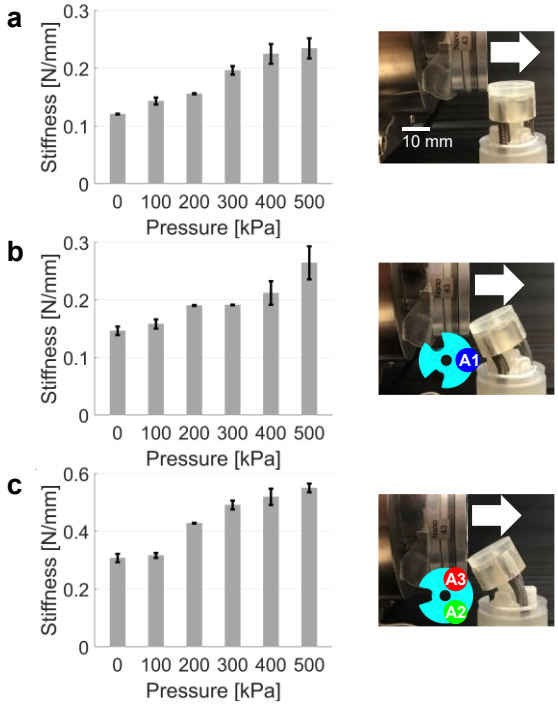

Fig. 9. Stiffness results at different input pressures of the soft pads while the module was at: (a) 0° initial position (no pressure at the spring-reinforced actuators); (b) 30° initial position by pressurizing the A1 actuator; (c) 30° initial position by pressurizing the A2 and A3 actuators, simultaneously. Each configuration was tested 5 times. The white arrows show the direction of the force sensor moved by a robot arm.

E. Integration of Multiple Modules

As described in Section II-A, a soft continuum manipulator with an articulated variable stiffness structure can be obtained by integrating *n* modules in a snake-like configuration, reducing the number of the required pneumatic tubes from *4n* to *n + 3* (i.e., three for the actuation and one for the stiffness modulation of each joint). The tubes of the spring-reinforced actuators of each module (A1, A2, and A3 in Fig. 2) are serially integrated. As a consequence, the modules are dependent on each other. On the other hand, the variable stiffness mechanism is the key feature to make each module independent. Thus, each module has its own stiffness tube (VS1, VS2, and VS3 in Fig. 2 where

n = *3*). This allows for controlling the motion freedom of each segment upon pressurization. For example, when the stiffness of Module 2 is increased through pressurizing VS2, and then one of the actuators (e.g., A1, A2, or A3) is pressurized, the bending of Module 2 would be less than the bending of Module 1 and Module 3.

As a demonstration, three modules were integrated by using a total of six pneumatic tubes (Fig. 10 and Supplementary Video 3). Two spacer disks were used to allow for pressure transmission among the spring-reinforced actuators. Since each joint was designed to bend up to 30° omnidirectionally, the multifunctional manipulator can bend up to 90° omnidirectionally (Fig. 10b-e). However, using the variable stiffness mechanism, it is possible to achieve also double curvature configurations by a proper pressurization sequence of actuators and variable stiffness mechanisms (Fig. 10f and g).

The proposed concept allows for a reduction in the overall number of fluidic tubes required by adding a new module. Indeed, only one new tube per module is required for the variable stiffness joint. This represents an improvement with respect to some previous state-of-the-art solutions [4], [23]–[25]. In the future, a fully modular system could be achieved by using on board miniature valves and wireless sensor data transmission [13] [22]. In this scenario, the main challenge is related to the current mechatronic components available on the market for pneumatic actuation, which are heavy, bulky, and expensive. However, a promising solution for fully integrated modular systems is the use of soft valves that can control airflow by acting as switches for automated functions in soft pneumatic circuits [26], [27].

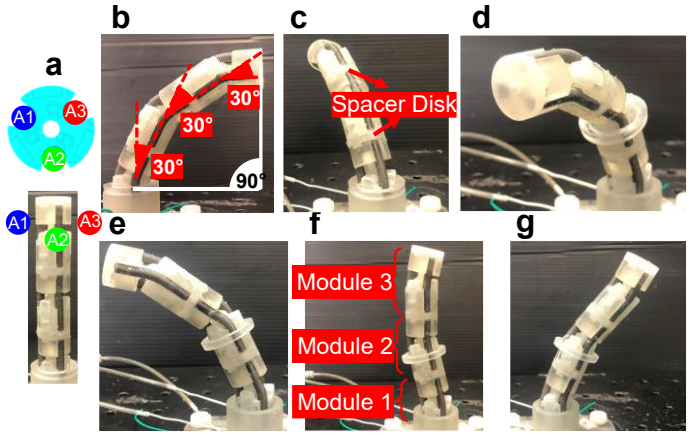

Fig. 10. Manipulator with three modules: (a) 0° initial position (no pressure at the actuators); (b) A1, (c) A2, and (d) A3 was pressurized, respectively; (e) A2 and A3 were pressurized simultaneously. To achieve the shape in (f): *i*) A2 and A3 were pressurized, *ii*) the soft pads of Module 1 were pressurized, *iii*) A2 and A3 were depressurized, *iv*) A1 was pressurized. To reach the shape in (g): *i*) A1 was pressurized, *ii*) the soft pads of Module 1 and 2 were pressurized, *iii*) A1 was depressurized, *iv*) A2 and A3 were pressurized.

The module is presented as a general-purpose technology. Indeed, it can be adapted to a wide range of applications from medical to aerospace [28]. To assess the capability of the module to operate in potential application scenarios, we exploited a manipulator made of three modules for performing standard medical tasks. Indeed, given the (1) working channel at the center, (2) the capability to perform complex movements in the 3D space, and (3) to increase the stiffness up to 95%, this solution might be advantageously used for a set of medical tasks. For instance, a needle for biopsy or a gripper can be steered by the manipulator (see Fig. 11 and Supplementary Video 3).

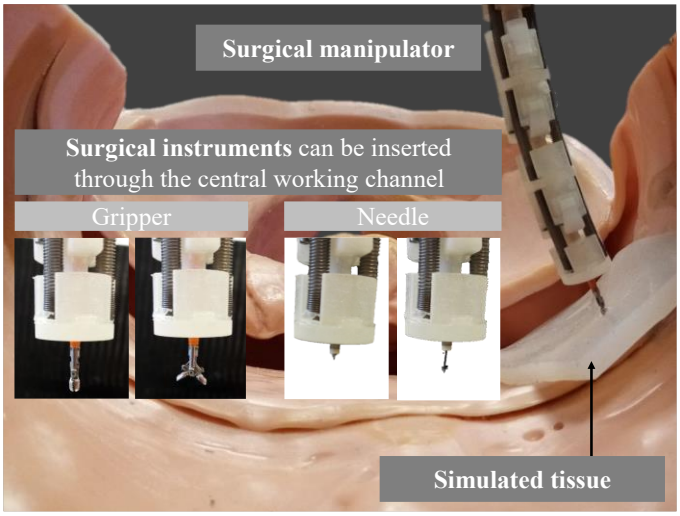

Fig. 11. *In silico* surgical procedure task by using the proposed manipulator. Different surgical instruments, such as grippers or needles, can be steered by the manipulator exploiting the central working channel.

IV. Conclusion

This study presents a compact and lightweight module with a hybrid soft-rigid structure that combines actuation, proprioceptive sensing, and variable stiffness. It is composed of a rigid mechanical structure, compliant metallic springs, and soft actuators. Three pressure-controlled spring-reinforced soft actuators were used to control the position of the module in the 3D space. Upon pressurization, the inductance of each spring changes, allowing for module position sensing. Finally, pressure-controlled soft pads, equally distributed around a central rigid ball joint, allow for controlling the module stiffness regardless of its position.

The characterization of a single module was carried out by investigating: *i*) the tip position and force output at different input pressures of the actuators; *ii*) sensor outputs at different bending angles; *iii*) variable stiffness capability at different input pressures of the soft pads. Then, a demonstration of the feasibility of a closed-loop position control was reported.

Finally, three modules were integrated serially to develop a continuum soft manipulator with an articulated variable stiffness structure. The proposed architecture allows for a reduction in the number of pneumatic tubes required by adding a new module from $N_t = 4n$ to $N_t = 3 + n$.

In terms of workspace, when each spring-reinforced actuator was pressurized one by one at the same pressure, the bending angle of the module showed differences (i.e., 30°, 27°, and 27°, at 130 kPa, Fig. 4). This could be due to some differences during the manufacturing and the installment of the soft actuators. The integration of multiple modules allows for enlarging the workspace, as shown in Fig. 10 and Supplementary Video 3.

As usual in soft actuators [29], hysteresis phenomena were observed in the bending angle of the module after different cycles of pressurizations and depressurizations (see

Supplementary Video 3). This is mainly due to the inherent behavior of soft materials like silicone and to the frictional forces between the rigid parts of the spherical joint. However, in the proposed solution, the final module position can be controlled by regulating the inlet pressure of the three actuators, based on the spring sensors signals, thus reducing the issue of hysteresis in the system control. For example, in case the module is not able to recover the initial position during depressurization, the spring sensors allow for pointing out the wrong position and the antagonistic actuators can be activated to reach the desired position [21].

Regarding the output force, the actuators generated similar values with slight differences, which could be due to hand-made fabrication as well (Fig. 5). The initial positions (0° and 30°) did not show a major effect on output forces.

The proposed variable stiffness mechanism demonstrated promising results, allowing for an increment of the stiffness up to 95% (Fig. 9). Further optimization in the material of the soft pads and geometry of the ball joint dents could allow for achieving a full position locking. In addition, the variable stiffness mechanism is the key feature to make each module autonomous from the others in the final manipulator. This allows for the control of the motion freedom of each joint, thus enabling more complex movements in the 3D space and reducing the number of pneumatic tubes.

The employed plastic material of the rigid parts (VisiJet M3 Crystal, 3D Systems, USA) was selected as a low-cost solution and it demonstrated to support up to 5 bar inlet pressure of the soft pads. However, a stiffer metallic material instead of a plastic one could be used in case higher stiffness is required, allowing further increment of the input pressure of the soft pads or the integration of stronger actuators. In addition, this material can suffer from long-term fatigue issues. Then, a more durable material can be selected based on the final application.

For the sensing part, the output voltage change of the spring sensors was characterized at different positions of the module (Fig. 6). For each sensor, the change in output voltage was large enough to detect the bending angle. By using these data, a closed-loop control was carried out in-plane. As shown in Fig. 7, a relatively higher error was found for small angles (i.e., 0° - 10°), probably due to friction phenomena.

REFERENCES

[1] W. Dou, G. Zhong, J. Cao, Z. Shi, B. Peng, and L. Jiang, "Soft Robotic Manipulators: Designs, Actuation, Stiffness Tuning, and Sensing," *Adv. Mater. Technol.*, vol. 6, no. 9, p. 2100018, Sep. 2021.

[2] C. Laschi, B. Mazzolai, and M. Cianchetti, "Soft robotics: Technologies and systems pushing the boundaries of robot abilities," *Science Robotics*, vol. 1, no. 1. American Association for the Advancement of Science, 06-Dec-2016.

[3] C. Zhang, P. Zhu, Y. Lin, Z. Jiao, and J. Zou, "Modular Soft Robotics: Modular Units, Connection Mechanisms, and Applications," *Adv. Intell. Syst.*, vol. 2, no. 6, p. 1900166, Jun. 2020.

[4] S. Kolachalama and S. Lakshmanan, "Continuum robots for manipulation applications: A survey," *J. Robot.*, vol. 2020, 2020.

[5] M. Manti, V. Cacucciolo, and M. Cianchetti, "Stiffening in soft robotics: A review of the state of the art," *IEEE Robot. Autom. Mag.*, vol. 23, no. 3, pp. 93–106, Sep. 2016.

[6] U. Culha, J. Hughes, A. Rosendo, F. Giardina, and F. Iida, "Design principles for soft-rigid hybrid manipulators," in *Soft Robotics: Trends, Applications and Challenges*, vol. 17, Biosystems and Biorobotics - Springer, Cham, 2017, pp. 87–94.

[7] F. Zhou, Z. Wu, M. Wang, and K. Chen, "Structure and mechanical properties of pincers of lobster (Procambarus clarkii) and crab (Eriocheir Sinensis)," *J. Mech. Behav. Biomed. Mater.*, vol. 3, no. 6, pp. 454–463, Aug. 2010.

[8] L. Paternò, G. Tortora, and A. Menciassi, "Hybrid Soft–Rigid Actuators for Minimally Invasive Surgery," *Soft Robot.*, vol. 5, no. 6, pp. 783–799, Dec. 2018.

[9] Y. Chen, S. Le, Q. C. Tan, O. Lau, F. Wan, and C. Song, "A reconfigurable hybrid actuator with rigid and soft components," *Proc. - IEEE Int. Conf. Robot. Autom.*, pp. 58–63, Jul. 2017.

[10] M. Su *et al.*, "Pneumatic Soft Actuator with Anisotropic Soft and Rigid Restraints for Pure in-Plane Bending Motion," *Appl. Sci. 2019, Vol. 9, Page 2999*, vol. 9, no. 15, p. 2999, Jul. 2019.

[11] E. Harsono, J. Yang, S. Bhattacharya, and H. Yu, "Design and analysis of a novel hybrid-driven continuum robot with variable stiffness," *Mech. Mach. Theory*, vol. 177, p. 105067, Nov. 2022.

[12] K. W. Kwok, H. Wurdemann, A. Arezzo, A. Menciassi, and K. Althoefer, "Soft Robot-Assisted Minimally Invasive Surgery and Interventions: Advances and Outlook," *Proc. IEEE*, 2022.

[13] M. A. Robertson and J. Paik, "New soft robots really suck: Vacuum-powered systems empower diverse capabilities," *Sci. Robot*, vol. 2, p. 6357, 2017.

[14] T. Kaufhold, V. Bohm, and K. Zimmermann, "Design of a miniaturized locomotion system with variable mechanical compliance based on amoeboid movement," *Proc. IEEE RAS EMBS Int. Conf. Biomed. Robot. Biomechatronics*, pp. 1060–1065, 2012.

[15] G. B. Crowley, X. Zeng, and H. J. Su, "A 3D Printed Soft Robotic Gripper with a Variable Stiffness Enabled by a Novel Positive Pressure Layer Jamming Technology," *IEEE Robot. Autom. Lett.*, vol. 7, no. 2, pp. 5477–5482, Apr. 2022.

[16] T. Liu, H. Xia, D. Y. Lee, A. Firouzeh, Y. L. Park, and K. J. Cho, "A positive pressure jamming based variable stiffness structure and its application on wearable robots," *IEEE Robot. Autom. Lett.*, vol. 6, no. 4, pp. 8078–8085, Oct. 2021.

[17] L. He, N. Herzig, S. De Lusignan, and T. Nanayakkara, "Granular Jamming Based Controllable Organ Design for Abdominal Palpation," *Proc. Annu. Int. Conf. IEEE Eng. Med. Biol. Soc. EMBS*, vol. 2018-July, pp. 2154–2157, Oct. 2018.

[18] C. Sozer, L. Paternò, G. Tortora, and A. Menciassi, "A Novel Pressure-Controlled Revolute Joint with Variable Stiffness," *https://home.liebertpub.com/soro*, Jul. 2021.

[19] C. Sozer, L. Paterno, G. Tortora, and A. Menciassi, "Pressure-Driven Manipulator with Variable Stiffness Structure," in *Proceedings - IEEE International Conference on Robotics and Automation*, 2020, pp. 696–702.

[20] I. Onda *et al.*, "Highly Articulated Tube Mechanism with Variable Stiffness and Shape Restoration Using a Pneumatic Actuator," *IEEE Robot. Autom. Lett.*, vol. 7, no. 2, pp. 3664–3671, Apr. 2022.

[21] S. K. Sahu, I. Tamadon, B. Rosa, P. Renaud, and A. Menciassi, "A Spring-based Inductive Sensor for Soft and Flexible Robots," *IEEE Sens. J.*

[22] G. Gerboni, T. Ranzani, A. Diodato, G. Ciuti, M. Cianchetti, and A. Menciassi, "Modular soft mechatronic manipulator for minimally invasive surgery (MIS): overall architecture and development of a fully integrated soft module," *Meccanica*, vol. 50, no. 11, pp. 2865–2878, Sep. 2015.

[23] B. T. Phillips *et al.*, "A Dexterous, Glove-Based Teleoperable Low-Power Soft Robotic Arm for Delicate Deep-Sea Biological Exploration," *Sci. Reports 2018 81*, vol. 8, no. 1, pp. 1–9, Oct. 2018.

[24] H. D. Yang and A. T. Asbeck, "Design and Characterization of a Modular Hybrid Continuum Robotic Manipulator," *IEEE/ASME Trans. Mechatronics*, vol. 25, no. 6, pp. 2812–2823, Dec. 2020.

[25] I. De Falco, M. Cianchetti, and A. Menciassi, "A soft multi-module manipulator with variable stiffness for minimally invasive surgery," *Bioinspiration and Biomimetics*, vol. 12, no. 5, p. 056008, Sep. 2017.

[26] P. Rothemund *et al.*, "A soft, bistable valve for autonomous control of soft actuators," *Sci. Robot.*, vol. 3, no. 16, Mar. 2018.

[27] S. V. Kendre *et al.*, "The Soft Compiler: A Web-Based Tool for the Design of Modular Pneumatic Circuits for Soft Robots," *IEEE Robot. Autom. Lett.*, vol. 7, no. 3, pp. 6060–6066, Jul. 2022.

[28] C. Zhang, P. Zhu, Y. Lin, Z. Jiao, and J. Zou, "Modular Soft Robotics: Modular Units, Connection Mechanisms, and Applications," *Adv. Intell. Syst.*, vol. 2, no. 6, p. 1900166, Jun. 2020.

[29] M. T. Thai, P. T. Phan, T. T. Hoang, H. Low, N. H. Lovell, and T. N. Do, "Design, fabrication, and hysteresis modeling of soft microtubule artificial muscle (smam) for medical applications," *IEEE Robot. Autom. Lett.*, vol. 6, no. 3, pp. 5089–5096, Jul. 2021.